Tellus (1990), *42A*, 444–462

The dynamics of coastal troughs and coastal fronts

By HANS ØKLAND, *Institute of Geophysics, University of Oslo, PO Box 1022 Blindern, 0315 Oslo 3, Norway*

(Manuscript received 7 November 1988; in final form 25 October 1989)

ABSTRACT

Mesoscale structures in the wind and pressure fields are demonstrated by case studies. Two main types are identified. The one is characteristic for the coast of Northern Norway and is called coastal trough in this paper. The other, typical for the south-eastern coast, has similarities to the New England phenomenon named coastal front. Both occur during the winter season. The structures are quasi-permanent in certain weather conditions, which suggests a description in terms of a stationary model in two space dimensions, assuming that the variables do not change in a direction parallel to the straight coastline. The scaled equations depend on two non-dimensional numbers, which in general are small, permitting a series expansion of the perturbation variables. Solutions of zero and first order are derived, essentially by analytical methods. The size and structure of the solutions are compared to the case studies. The results seems to verify the initial hypothesis, namely that the trough is caused mainly by differential heating, while the front also depends on the discontinuity in surface friction.

1. Introduction

It is the intention of this paper to study certain characteristic wind perturbations often noted along the coast of Norway during the cold season. We suspect that such phenomena exist in other parts of the world as well, but we have little knowledge of their climatology. However, one type, which we characterize as a front, has been studied extensively at the coast of New England. It will be shown that some main characteristics of the phenomena may be investigated in terms of a two-dimensional, stationary model. We shall principally use analytical methods, rather than numerical integrations. In our opinion this gives greater insight into the general kinematics and dynamics of the perturbations, although some rather drastic simplifications will be necessary. The model is described in Section 2, but first the main characteristics of the phenomena will be demonstrated by two case studies.

The trough is noticed on surface weather maps when a cold air mass, originating over the ice-covered polar region, flows across the waters of the Norwegian Sea towards the coast (Fig. 1). The most obvious consequence of the trough is to maintain strong winds over the sea, while the wind force is moderate over land. On the special occasion pictured, this is specifically obvious between 10°E and 30°E.

Usually, an outbreak of cold air follows the passage of a cyclone. Sometimes the cyclone continues to move eastward and weakens, resulting in a rapid decrease in the cold air flow. In such cases, the trough is weak or does not develop at all. On other occasions the low is retarded or comes to rest over the Barents Sea. Then the trough is usually well developed and may last for days.

Fig. 2 shows the 700 mb map 3 hours later. The reason why we did not use the surface weather map for the same time as the 700 mb map is that two ship observations off the coast were missing. There are strong winds west of about 10°E, associated with an approaching polar front disturbance. East of this longitude the 700 mb wind is not so strong as the surface wind, and of a more northerly direction. As far as one can judge from

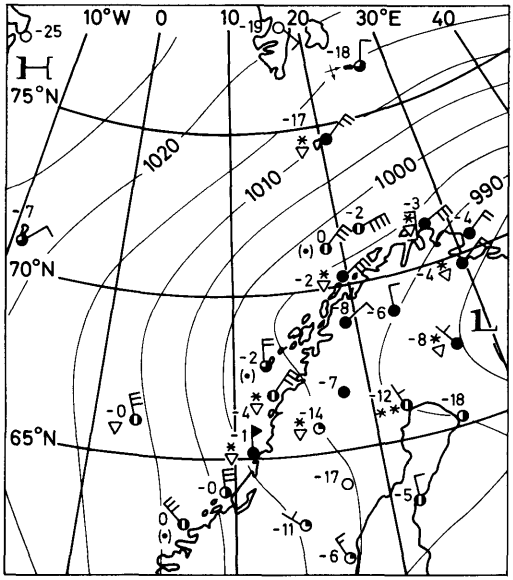

Fig. 1. Surface weather map for 3 December 1980, 0900 GMT, showing coastal trough over Northern Norway. Barbs on wind arrows indicate 5 m s^{-1} (long) and 2.5 m s^{-1} (short).

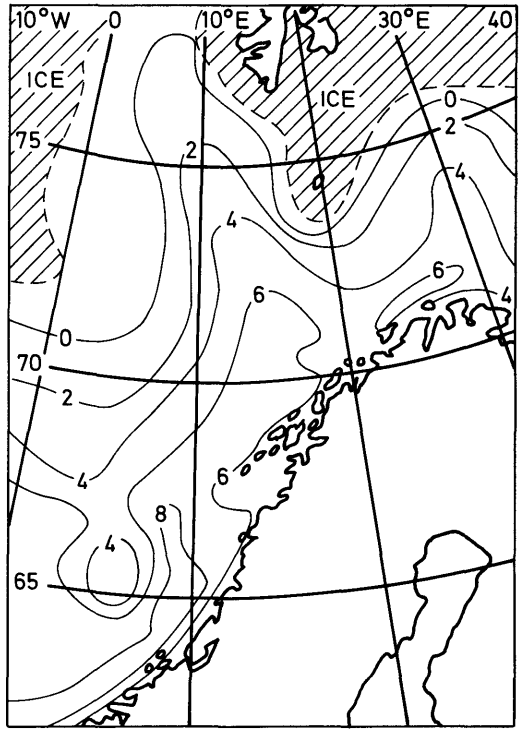

Fig. 3. Sea surface temperature and extension of sea ice on 4 December 1980.

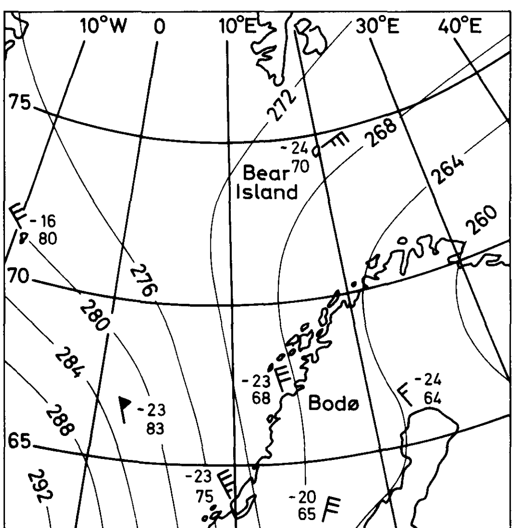

Fig. 2. The 700 mb map for 3 December 1980, 1200 GMT. Plotting convention for winds as in Fig. 1.

the sparse observations, there are few signs of a coastal trough at this level, although there is some vorticity on a larger scale associated with the polar front cyclone.

The source area for the cold aiı mass is quite uniform. This is also true for the air mass when it enters the ocean, at least in its lower part which is very cold and very stable (Fig. 4, left sounding). At the edge of the ice the air enters the open waters with a sea surface temperature exceeding the air temperature by more than 20°C (Fig. 3). This leads to rapid heating which continues until the air reaches the snow-covered continent (Fig. 4, right sounding). There the strong turbulent heat flux stops, and changes in the temperature are brought about by slower processes, mainly radiation.

Heating from below of a stably stratified air mass inevitably leads to the formation of a convective layer, usually capped by an inversion. This is, in fact, indicated by the right hand

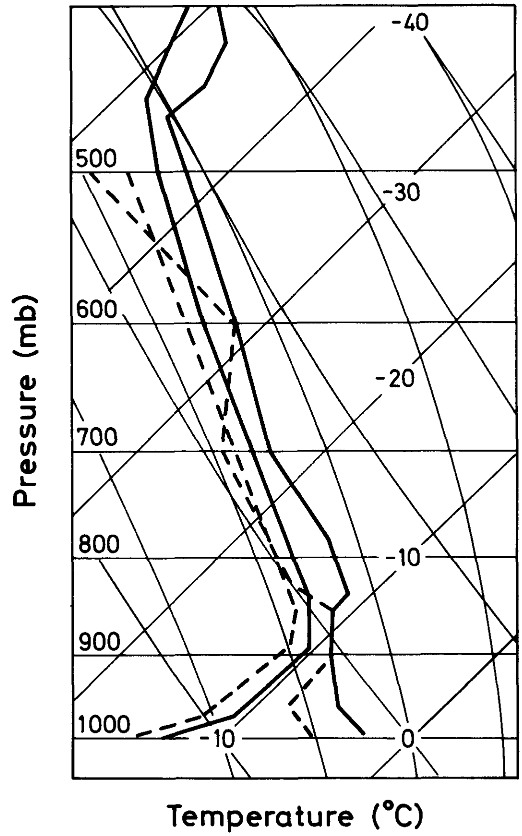

Fig. 4. Temperature and dewpoint soundings on 3 December 1980. Left soundings from Bear Island (74.30° N, 19.00° E), 0000 GMT, and right soundings from Bodø (67.18° N, 14.20° E), 1200 GMT.

sounding on Fig. 4, although not quite clearly because of the fact that the layer between 960 mb and 850 mb is slightly stable in the moist adiabatic sense. We believe that this is either erroneous or of strictly local character. (The observing station Bodø is located in the mouth of a long and narrow fjord surrounded by mountains.) In fact, we are convinced that the lapse rate over the open sea is unstable up to the 850 mb level. We find support for this belief in the circumstance that the upper part of the layer is saturated with water vapour according to the sounding, and that snow showers are reported along the coast (Fig. 1). In fact, the condensation level is probably at 960 mb. Furthermore, many other case studies show the convective layer quite clearly. Finally, evaluations based on methods presented elsewhere (Økland, 1983) indicate that the convective layer depth should be about this size under the existing conditions.

Generally speaking, the important dynamical factor is the differential heating, and not the heating per se. Therefore, it is our hypothesis that the abrupt change in the rate of heating produces the trough, and we shall show that this hypothesis leads to a disturbance of the right structure and magnitude. However, other factors like mountains and friction may have a modifying influence. This will be studied more closely in due time.

A different wind pattern is pictured in Fig. 5, showing a surface weather map covering the Skagerrak and surrounding parts of Norway, Sweden and Denmark. The numbers with decimal points are the 12 h precipitation in mm. The other symbols are standard. Here again we see a trough which is especially sharp along the south-eastern coast of Norway facing Skagerrak. The situation is different from the previous one in that the air which flows towards the coast is not particularly cold, and the heating produced by the open waters of Skagerrak is weak. The coldest air is over land, and may in part be advected from north-east over the cold continent. The inversion appearing on the temperature soundings (Fig. 6) is associated with a deep quasi-stationary front. The surface front is located just south of the map section shown in Fig. 5.

This weather situation is similar to one described by Bergeron (1949) and pictured by him as a composite map for a period of several days. Bergeron points to the maximum of precipitation just along the coastline. He also points to the coast of New England and predicts that "very pronounced coastal snow-maxima must sometimes form in this region". And, indeed, this has been shown to be the case, as demonstrated by Bosart et al. (1972) and Bosart (1975). The name "coastal front" was not used by Bergeron. In fact, the classification of this rather shallow phenomenon as a front is somewhat dubious. However, it has later come into use for the New England type, and it will also be used in this paper.

We have found that this second wind structure, although apparently different from the first one, may be studied by essentially the same model. It has been discovered that the North American

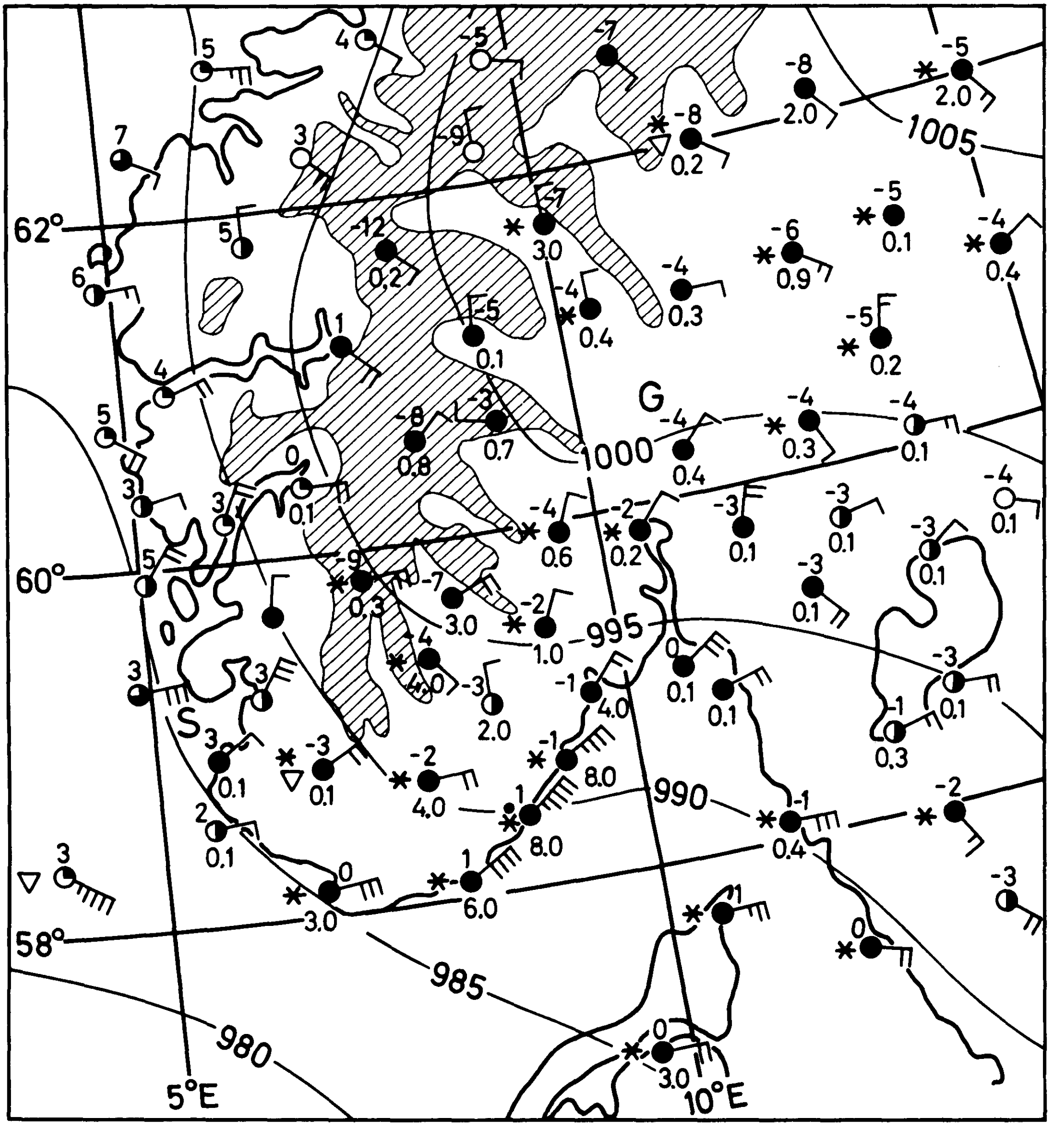

Fig. 5. Surface weather map for Southern Norway on 30 January 1988, 0600 GMT. Numbers with decimal point are 12 h precipitation in mm. The hatched region is above 500 m.

type is associated with heating of very cold air which is brought southward over the Atlantic where it is rapidly heated (Ballentine, 1980). Then, on returning to the coast of New England, the heating suddenly stops. This is quite in agreement with what we have taken as the starting point for the coastal trough at the coast of Northern Norway. The case described along the south-eastern coast is somewhat different, since the heating probably is less important. Instead, the difference in friction over the land and the sea may be the predominant factor. This was mentioned by Bergeron (1949), and will also be studied in the context of the model we shall use. Again, we stress the simplification which is necessary in order to carry out the theoretical

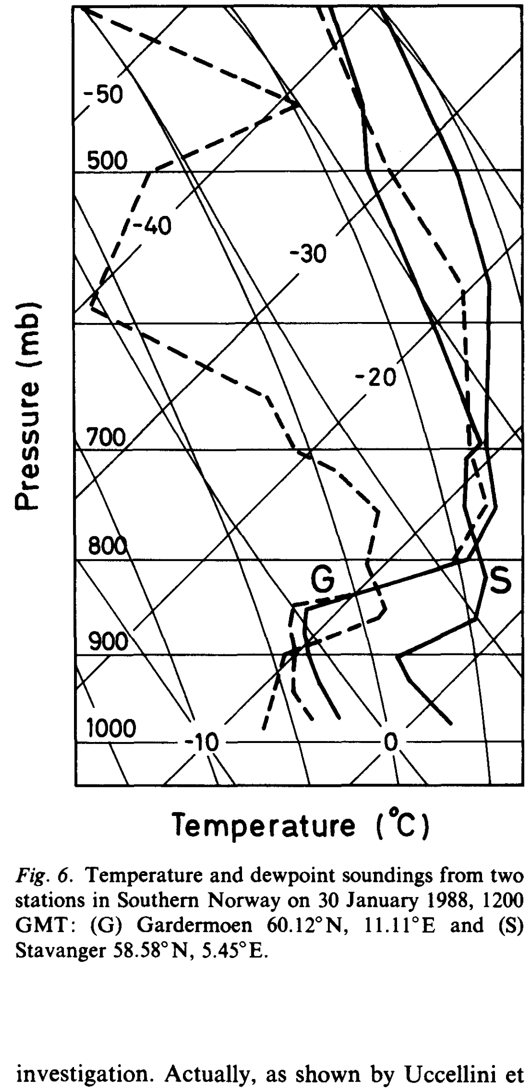

Fig. 6. Temperature and dewpoint soundings from two stations in Southern Norway on 30 January 1988, 1200 GMT: (G) Gardermoen 60.12°N, 11.11°E and (S) Stavanger 58.58°N, 5.45°E.

investigation. Actually, as shown by Uccellini et al. (1987), the New England frontogenesis may be a complicated interaction between an upper air disturbance and the low level temperature contrast. Nevertheless, we hope to shed light upon certain aspects of the phenomenon. Many of the results agree with Bosart's (1975) analysis.

Section 2 contains the main model studies. Specifically, the model equations are derived in Subsection 2.1 while the series expansion and the solutions are developed in the following subsections. Section 3 is devoted to the influence of the topography and friction. Section 4 contains some final remarks. A note about the heating of a moist convective layer is added as an Appendix.

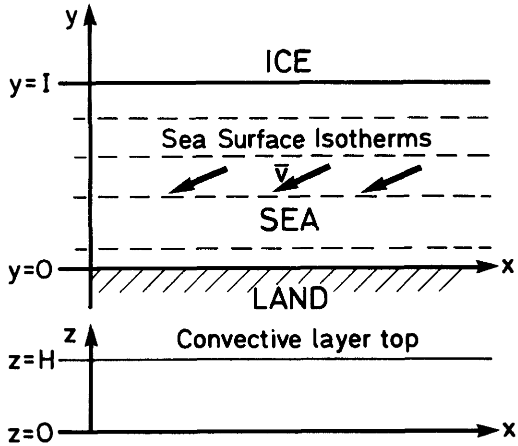

Fig. 7. The structure of the model. See text for further explanation.

2. The model

We assume a barotropic basic state characterized by the constant geostrophic wind, $\bar{\boldsymbol{v}} = (\bar{u}, \bar{v})$, and the potential temperature distribution $\bar{\theta} = \theta_r + \Gamma z$, where θ_r is a reference value and Γ the constant vertical lapse rate of potential temperature. Superimposed upon this basic state we postulate a perturbation caused by the difference in the rate of heating as the air is advected by the basic state wind from the warm ocean to the cold continent. The height of the perturbation, H, is considered to be constant. We place the x-axis along the straight shoreline with the y-axis pointing towards the sea, and assume that $\bar{v} < 0$. The perturbation variables will be restricted to vary only with the y and z coordinates. We shall search for stationary solutions of the perturbation equations, forced by $\bar{v}$ and the differential heating.

This perturbation problem corresponds to the idealized case pictured in Fig. 7. A horizontally homogeneous cold air mass enters the sea at $y = I$, assumed for instance to be the edge of ice-covered ocean. Over the water the air is heated by turbulent fluxes, leading to the formation of a convective layer. This is the part of the atmosphere affected by the heating. Accordingly, we postulate that the perturbation in its broad feature is confined to this layer so that the scale height, H, is the characteristic value of the convective layer depth. We shall comment on this assumption on a couple of occasions.

The thickness and temperature of the convective layer increase downstream, quite rapidly close to the ice edge, but more slowly as the layer becomes thicker. However, for simplicity the height of the model will be treated as a constant. Similarly, the basic state lapse rate, Γ, will be a constant overall lapse rate of the convective layer. The model assumption of no variation in the direction of the x-axis, is supported by the observed fact that the sea surface isotherms are largely parallel to the coast (Fig. 3).

The basic state wind component parallel to the coast interacts with the perturbation only through the surface boundary conditions. As the wind speed increases the turbulent fluxes of heat and momentum become larger. However, in our model formulation we make no attempt to parameterize the heat flux. Instead, we prescribe the heating as a function of y. The momentum flux, however, will be parameterized by means of Ekman layer theory, making it a function of the surface wind and the drag coefficient.

Apart from turbulent fluxes of sensible and latent heat there may be other heat sources, primarily radiation. We shall here consider them to be of minor importance.

2.1. *The perturbation equations*

Based on the description of the model above, the Boussinesq approximation and the quasi-static assumption, the equations governing the perturbation may be written

$$v_y + w_z = 0, \tag{1a}$$

$$\bar{v}u_y + vu_y + wu_z - fv = 0, \tag{1b}$$

$$(\bar{v}v_y + vv_y + wv_z)_z + fu_z + (g/\theta_r)\theta_y = 0, \tag{1c}$$

$$\bar{v}\theta_y + \Gamma w + v\theta_y + w\theta_z = Q/c_p. \tag{1d}$$

Here (u, v, w) is the perturbation velocity and θ the departure of potential temperature from $\bar{\theta}$. The hydrostatic equation (not shown) has been used to eliminate the pressure perturbation from the y component of the momentum equation. In eq. (1d), Q/c_p is the heating rate per mass unit of air, times $(p_r/p)^\gamma$, where p_r is a reference pressure and $\gamma = R/c_p$. Since the heating per definition is produced by the turbulent flux, F_H, we have the relation

$$F_H = \int_0^H Q\varrho_r \, dz, \tag{1e}$$

where ϱ_r is a constant mean value of density. In the equations the perturbation is described in terms of the "internal" variables u, v, w and θ, while the forcing from the basic state is introduced by "external" variables, primarily $\bar{v}$, Γ, H and Q. Some insight into the structure of the perturbation is provided by a careful scaling of the equations. Successive approximations to a solution will then be worked out from the non-dimensional equations by series expansion in terms of two small non-dimensional numbers.

The obvious scale for z is H, or a length of comparable size. The horizontal length scale, L, presumably depends on the width of the area with appreciable variation in the heating rate. However, since it turns out that the appropriate solution has a quasi-geostrophic character, the problem has an intrinsic scale, the Rossby radius of deformation, which determines the dimension of the perturbation for a sufficiently narrow zone of variation in the heating rate. This will be demonstrated in the following analysis. For the present we postulate that $L = HN/f$, where N is the buoyancy frequency, defined by $N^2 = g\Gamma/\theta_r$.

There are three horizontal velocity components in the equations; $\bar{v}$, u and v. Since there is no a priori reason why they should be of the same characteristic size, we postulate separate scales, U and V, for u and v, while $\bar{v}$ is scaled by its own absolute value. We shall presently derive a relation between these three scales, but first we note that eq. (1a) is scaled as follows

$$v_y + \frac{WL}{VH} w_z = 0, \tag{2a}$$

where W is the scale for w and where we have neglected the usual primes to indicate non-dimensional variables. Choosing $W = VH/L$, the scaled version of eq. (1b) becomes

$$-\varepsilon \frac{|\bar{v}|}{V} u_y + \varepsilon(vu_y + wu_z) - v = 0, \tag{2b}$$

where the leading minus sign comes from the fact that $\bar{v}$ is assumed to be negative in all applications. The number $\varepsilon = U/(fL)$ will be termed the internal Rossby number for the perturbation.

Note, however that with $L = HN/f$, ε turns out to be identical to the Froude number, $U/(HN)$. At this point we postulate $\varepsilon \ll 1$. Later on we shall derive conditions for this to be true. Then, since the first and the last term must both be O(1), the relation $V = \varepsilon|\bar{v}|$ is suggested. Using this result the third equation becomes

$$-\delta v_{yz} + \delta\varepsilon(vv_y + wv_z)_z + u_z + M\theta_y = 0, \tag{2c}$$

where

$$M = \frac{g}{\theta_r}\frac{HT}{fUL}.$$

Here $\delta = \bar{v}^2/(fL)^2$, and T is the scale for θ. The number $\delta^{1/2}$ will occasionally be referred to as the external Rossby number. If both ε and δ are small numbers, the equation obviously is an approximation to the thermal wind equation. Therefore, a natural assumption is $M = 1$, which establishes a relation between U and T.

Finally, the fourth equation is written in non-dimensional form as

$$-\theta_y + s^2 w + \varepsilon(v\theta_y + w\theta_z) = q, \tag{2d}$$

where

$$s^2 = \frac{N^2 H^2}{f^2 L^2}, \tag{3a}$$

$$q = \frac{Q}{c_p}\frac{L}{|\bar{v}|\,T}, \tag{3b}$$

and where we have used the previous assumptions $V = \varepsilon|\bar{v}|$ and $M = 1$. Note that the scaled value of F_H, according to eq. (1e) may be written as

$$\sigma = \int_0^1 q\,dz = \frac{F_H}{c_p H \varrho_r}\frac{L}{|\bar{v}|\,T}. \tag{4}$$

The quantity $|\bar{v}|\,T/L$ is seen to be a measure of the temperature change produced by advection in the basic state wind field $\bar{v}$. Note that $s^2 = 1$ when $L = NH/f$, the Rossby radius.

With the first two terms in eq. (2d) of magnitude one and the third much smaller, the magnitude of the last term may be no larger than of unity, and in general smaller since the two first terms mostly are of opposite sign. Consequently, we may assume that the characteristic change in the heating rate across the coast, Q^*/c_p, say, is at most of the same order of magnitude as $|\bar{v}|\,T/L$. Combining with the previous assumptions $M = 1$ and $L = NH/f$, we then derive the relation

$$\varepsilon = \frac{L}{|\bar{v}|\,H\Gamma}\frac{Q^*}{c_p}. \tag{5}$$

Eq. (5), concludes the search for the appropriate scales and establishes a relation between the strength of the perturbation, measured by ε, and parameters for the external forcing; $|\bar{v}|$ and Q^*. The condition for ε to be small may be written as

$$\frac{Q^*}{c_p} \ll H\Gamma|\bar{v}|/L. \tag{6}$$

where $L/|\bar{v}|$ is the advective time scale and ΓH measures the vertical temperature difference. This condition, together with $\delta \ll 1$, form the basis of the scaling and is necessary in order to study the solution by series expansion in terms of ε and δ. Of course, the argumentation by no means excludes perturbations also when ε, δ or both are of order one or larger. What happens in this case is not so easily seen. Note, however, that the rate of heating is fairly well established on the basis of the sea surface temperature, the height and temperature of the convective layer etc., while $|\bar{v}|$ may vary within wide limits. Then, according to eq. (5), ε and $\delta^{1/2}$ tend to be inversely proportional, indicating that a large $|\bar{v}|$ gives a small perturbation. This is in good agreement with observations, and, in fact, is also seen in Fig. 1 and Fig. 2, where the value of the on-shore geostrophic wind is strong south of 65°N, where the perturbation appears to be weak.

In the following example, we have taken values from the first case study. They are $\Gamma = 0.003$ K m^{-1}, $f = 1.35 \times 10^{-4}$ s^{-1} and $H = 1300$ m. We then get $N = 10^{-2}$ s^{-1} and $L = 100$ km. With $|v| = 7$ m s^{-1}, δ turns out to be $\frac{1}{4}$, and $H\Gamma|\bar{v}|/L = 2.6 \times 10^{-4}$ K s^{-1}. We compare this value to the heating rate produced by the flux, F_H, from the ocean

$$Q^*/c_p = \frac{F_H}{c_p \varrho H},$$

and utilize the so-called bulk formula

$$F_H = \varrho c_p C_H |\boldsymbol{v}|\,\Delta T.$$

With the coefficient of heat transfer $C_H = 1.4 \times 10^{-3}$, $|\boldsymbol{v}| = 15$ m s^{-1} and the temperature difference between air and sea surface, $\Delta T = 8$ K, we get $Q^*/c_p = 1.3 \times 10^{-4}$ K s^{-1} = 11 K Day^{-1}, which according to eq. (5), gives $\varepsilon = \frac{1}{2}$.

2.2. *Series expansions of a solution*

Eqs. (2a)–(2d) may be written in a slightly different form:

$$v_y + w_z = 0, \tag{7a}$$

$$-u_y + \varepsilon(vu_y + wu_z) - v = 0, \tag{7b}$$

$$-\delta v_{yz} + \delta\varepsilon(vv_y + wv_z)_z + u_z + \theta_y = 0, \tag{7c}$$

$$-\theta_y = \varphi, \tag{7d}$$

$$\varphi = q - w - \varepsilon(v\theta_y + w\theta_z), \tag{7e}$$

where φ is a new variable which will be explained presently. In passing we note that ε measures the influence of the non-linear terms, while the terms containing δ, and especially the first one, represent deviations from the geostrophic balance by terms like $\bar{v}\theta_y$ (cf. eq. (1c)).

We now take advantage of the fact that in the convective layer the vertical temperature lapse rate is close to the adiabatic one. In the case under investigation here, this usually means that a dry adiabatic stratification is found below the condensation level while the upper part adjusts to the saturated adiabat. In fact, it has been implicitly assumed that a considerable part of the model depth is above the condensation level. Dry convection through the whole layer would make $(\Gamma + \theta_z)$ very small (actually slightly negative) and thus invalidate the scaling assumptions.

In the case of moist convection $(\Gamma + \theta_z)$ is no longer independent of z. However, we are free to choose Γ as a constant measure of the mean stability. In addition, we shall here use the approximation that $\theta_z = 0$ through the whole model domain. In that case φ, defined by eqs. (7d) and (7e) must be a function of y only.

That the convection restricts the heating in a way similar to the one indicated above, is easily understood. For instance, if the two last terms in eq. (7e) should produce a stabilization above a certain height, the layer below this height would be heated but not the layer above, and the stable stratification would soon be removed. Therefore, all parts of the convective layer must be heated as long as the heat flux from the sea is maintained. However, the potential temperature will not increase by the same amount at all heights, as postulated above. The reader may find a closer examination of this approximation in the Appendix. There we conclude that the error is tolerable in the actual case. The constraint in eqs. (7d) and (7e) will be used in the following to construct an equation which determines φ. A similar approach has been used by this author in a previous study (Økland, 1987).

Solutions to eqs. (7a)–(7e), if any, must be functions of ε and δ. If these numbers are small, the variables may formally be expanded in power series. We begin with ε, and write the variable u as

$$u = u_0 + \varepsilon u_1 + \cdots,$$

and similarly for the other variables. It will prove to be convenient at this stage to change the vertical scale from H to H/c where $c = 2\sqrt{3}$.

Inserting the series into eqs. (7a)–(7e) and collecting zero order terms, we get

$$v_{0y} + w_{0z} = 0, \tag{8a}$$

$$-u_{0y} - v_0 = 0, \tag{8b}$$

$$-\delta v_{0yz} + u_{0z} + \theta_{0y} = 0, \tag{8c}$$

$$-\theta_{0y} = \varphi_0(y), \tag{8d}$$

$$\varphi_0(y) = q_0 - w_0. \tag{8e}$$

From eqs. (8a)–(8d), one derives the following equation:

$$w_{0zz} + \delta w_{0yyzz} = \varphi_0'', \tag{9}$$

where φ_0'' is the second derivative of φ_0. At the present stage we use at the horizontal boundaries the conditions

$$w_0(z = 0) = w_0(z = c) = 0, \tag{10}$$

in which case eq. (9) may be written as

$$w_0 + \delta w_{0yy} = \tfrac{1}{2}z(z - c)\varphi_0''. \tag{11}$$

Clearly, the upper boundary condition has the consequence that the heating and the forced vertical circulation is confined to the same layer. The lower boundary condition will be modified later when we study the influence of surface friction and variable terrain height, and we shall also comment upon the upper boundary condition for that case.

We now get from eq. (11):

$$\left(1+\delta\frac{d^2}{dy^2}\right)\int_0^c w_0\,dz = -c\varphi_0'', \tag{12}$$

taking into account that $c = 2\sqrt{3}$. Similarly, from eq. (8e)

$$c\varphi_0 = -\int_0^c w_0\,dz + \sigma_0, \tag{13}$$

where

$$\sigma_0(y) = \int_0^c q_0\,dz \tag{14}$$

represents the heat flux as in eq. (4). Elimination of w_0 from eqs. (12) and (13) gives

$$(1-\delta)\varphi_0'' - \varphi_0 = -\frac{1}{c}(\sigma_0 + \delta\sigma_0''). \tag{15}$$

From this second-order ordinary differential equation, φ_0 may be derived provided σ_0 is known and certain boundary conditions are determined. We shall assume that φ_0 is finite everywhere and, in agreement with σ_0, vanishes for large negative values of y.

There is a certain arbitrariness in the choice of lateral boundary conditions. The mathematical problem needs boundary conditions at two distinct values of y. However, for physical reasons we do not want to formulate conditions which impose too rigorous constraints on the solution, since the objective is to study the influence of the coast. A vanishing perturbation at $y = -\infty$ seems natural in the case under consideration. Earlier in this study we postulated an ice-edge at $y = I$, introduced as a limit of the horizontally homogeneous arctic air mass (Fig. 5). It is clear that the ice-edge can create a perturbation which is a mirror of the perturbation at the coast. Also, if the latter has an asymptotic value for increasing y, and the former a similar one for decreasing y, the two will approximate each other in the middle of the ocean.

2.2.1. Asymptotic solution for $\delta \to 0$. If $\delta \ll 1$, u_0, u_1 etc. may be expanded in series containing terms with increasing powers of δ, like

$$u_0 + u_{00} + \delta u_{01} + \cdots. \tag{16}$$

Collecting zero-order terms we now get the following set of equations:

$$v_{00y} + w_{00z} = 0, \tag{17a}$$

$$-u_{00y} - v_{00} = 0, \tag{17b}$$

$$u_{00z} + \theta_{00y} = 0, \tag{17c}$$

$$-\theta_{00y} = \varphi_{00}(y), \tag{17d}$$

$$\varphi_{00}(y) = -w_{00} + q_{00}, \tag{17e}$$

$$\varphi_{00}'' - \varphi_{00} = -\frac{1}{c}\sigma_{00}. \tag{17f}$$

Note that eq. (17c) shows a perfect geostrophic balance at this level of approximation. The equations describe an *asymptotic* solution for $\delta \to 0$. However, δ exactly equal to zero means that $\bar{v} = 0$. Then, the first term in eqs. (17b) and (17d) should also be neglected, and the solution is trivial.

A solution to eq. (17f) may be given as

$$\varphi_{00} = \frac{1}{2c}\int_{-\infty}^{\infty} e^{-|y-\eta|}\sigma_{00}(\eta)\,d\eta \tag{18a}$$

for any continuous or sectionally continuous function σ_{00}. The other variables are derived as follows

$$\theta_{00} = -\int_{-\infty}^{y} \varphi_{00}(\eta)\,d\eta, \tag{18b}$$

$$u_{00} = (z - c/2)\varphi_{00}, \tag{18c}$$

$$\psi_{00} = \tfrac{1}{2}z(z-c)\varphi_{00}', \tag{18d}$$

$$v_{00} = -\psi_{00z}, \tag{18e}$$

$$w_{00} = \psi_{00y}, \tag{18f}$$

where in eq. (18b) a constant of integration has been chosen in such a way that $\theta_{00}(-\infty) = 0$.

Note that eq. (17a) demonstrates what we have earlier referred to as the "intrinsic" scale. Each element of the forcing, $\sigma_{00}(\eta)\,d\eta$, is multiplied by a Green's function, $\exp|y-\eta|$, which has a characteristic scale of magnitude one, corresponding to the Rossby radius in dimensional space.

It is appropriate at this point to note some of the kinematic and dynamic characteristics of the perturbation as visualized by the system (eq. (17)). The interpretation is most clearly seen and understood on the basis of the equivalent dimensional system obtained by neglecting the non-linear terms in eqs. (1b) and (1d), and in (1c) the terms in parenthesis. Then, according to the simplified eq. (1d), the change in the rate of heating across the coastal area is balanced by the temperature advection in the basic state wind, $\bar{v}\theta_y$. Because of the geostrophic balance the temperature determines the wind component parallel to the coast, u. Furthermore, the momentum advection, $\bar{v}u_y$, balancing the Coriolis acceleration fv, determines the ageostrophic wind component across the coast. Finally, the vertical velocity derived from v takes part in the heat balance expressed by the dimensional equivalence to eqs. (17e) and (17f).

It is interesting to compare with quasi-geostrophic theory as described for instance by Eliassen (1959 and 1962). Following Eliassen (1962), the geostrophic relation is assumed to be valid also when its two terms are subject to the operator $\bar{v}\,\partial/\partial y$, actually an approximation to the material derivative based on the relation $V = \varepsilon|\bar{v}|$ derived earlier. Then, substituting for $\bar{v}u_y$ and $\bar{v}\theta_y$ from the simplified eqs. (1b) and (1d), one gets the above result. The basic difference from Eliassen's (1959) paper, which also deals with condensation, is our special formulation of the heating. In essence this formulation removes any vertical temperature difference produced by the vertical displacement.

As an example we choose

$$\sigma_{00} = 1 + \tanh y. \qquad (19)$$

This function, representing the flux of heat from the ocean, is seen to increase from zero at large negative values of y to 2 at large positive values. The smooth variation at $y = 0$ agrees with the fact that the sea surface temperature is lower in the coastal waters than at some distance from the coast (Fig. 3).

The integral eq. (18a) may then be solved exactly. One finds

$$\varphi_{00} = \frac{1}{c}\,(\mathrm{e}^{y} \arctan \mathrm{e}^{-y} - \mathrm{e}^{-y} \arctan \mathrm{e}^{y} + 1). \qquad (20)$$

The other variables are easily derived, using eqs. (18b)–(18f). Fig. 8 shows cross sections of ψ_{00}, u_{00} and θ_{00}. As might be expected, there is a closed circulation across the coast with rising motion over the ocean and sinking motion over the continent. The u_{00} field indicates cyclonic shear along the coast. Since u_{00} is geostrophic,

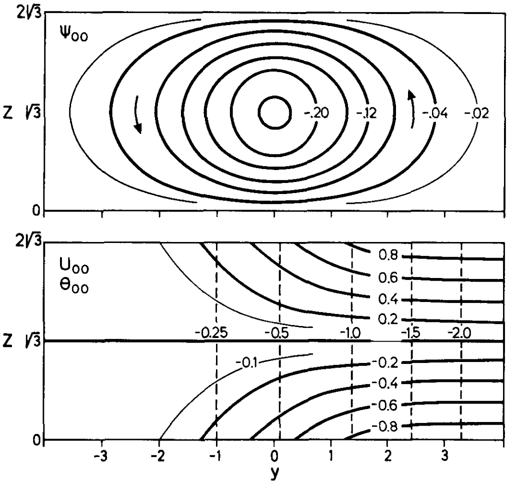

Fig. 8. Non-dimensional asymptotic solution of the perturbation equations. Top plate shows the stream function defining the vertical circulation across the coastline (i.e., the x-axis). Lower plate shows isolines for the velocity component parallel to the coast (full lines) and the perturbation temperature (broken lines). See text for further explanation.

the combined effect of u_{00}, $\bar{u}$ and $\bar{v}$ is a pressure trough. Using numerical values from Subsection 2.1, one gets the vorticity $Uu'_{00}(0,0)/L = 1.8 \times 10^{-5}\ \mathrm{s}^{-1}$. We have tried to determine a mean value of the relative vorticity along the coast between 10°E and 30°E from the pressure analysis on Fig. 1 and the height analysis on Fig. 2, using a "mesh width" of 150 km. The result is $2.6 \times 10^{-5}\ \mathrm{s}^{-1}$ on the surface map (Fig. 1) and $1.1 \times 10^{-5}\ \mathrm{s}^{-1}$ in the 700 mb surface (Fig. 2). The difference, $1.5 \times 10^{-5}\ \mathrm{s}^{-1}$, compares reasonably well with the theoretical value.

As a demonstration, we have prepared Fig. 9 where we have chosen $\bar{u} = 0$ and $\bar{v} = -U/2$. The lines are "isobars" derived from the geostrophic wind $(Uu_{00}(y,0), \bar{v})$.

It may seem surprising that the perturbation in the u_{00} field extends to infinity in the positive y direction. Also, at the height c, the perturbation velocity u_{00} is not zero, but equals the value at the sea surface with the opposite sign. Since the atmosphere above is assumed to be barotropic, the same perturbation must exist also here. On the other hand, the velocity component v_{00}, which is not geostrophic, may drop to zero at $z = c$. A physical "explanation" of these somewhat peculiar properties of the solution is the fact

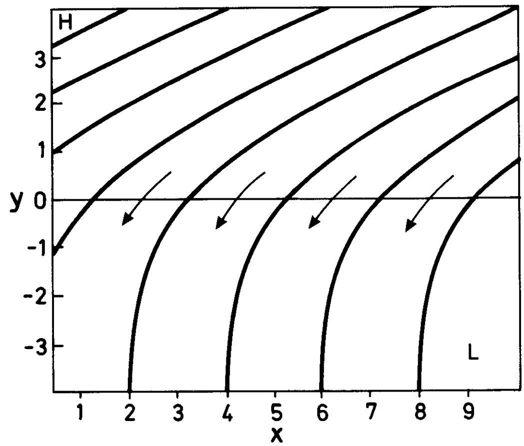

Fig. 9. An example of "surface isobars" defined by the geostrophic wind $(Uu_{00}(y, 0), -U/2)$. Here u_{00} is the non-dimensional perturbation wind parallel to the coastline and U is an arbitrary scale. The basic state wind is chosen as $(0, -U/2)$. See text for further explanations.

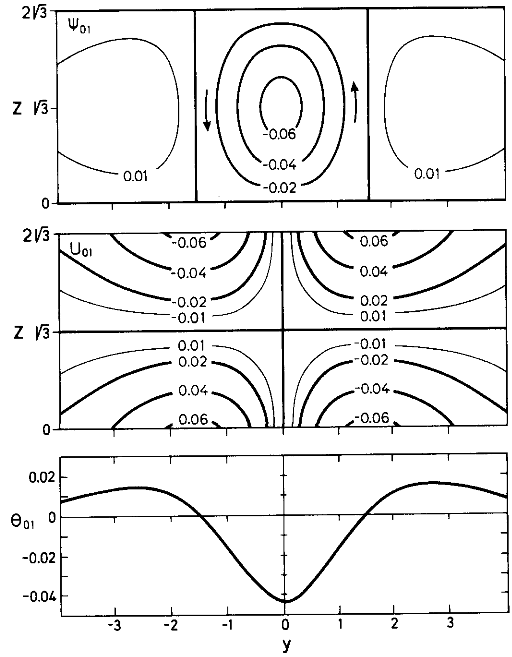

Fig. 10. First order solution in δ. The diagrams show stream function, velocity component parallel to coastline and potential temperature. Multiplied by δ, this solution is a correction to the asymptotic solution of Fig. 8.

that we have sought a stationary solution which might develop from a time-dependent model through an infinitely long time.

2.2.2. Approximate solution for $\delta \ll 1$. Turning now to the first order terms in the expansion (eq. (16)) one gets the following result, describing the modification of the previous asymptotic solution produced by the small non-geostrophic term, $-\delta v_{oyz}$, in eq. (8c). The case where this additional term has the same order of magnitude as the other terms is studied in Subsection 2.3.

$$\varphi''_{01} - \varphi_{01} = \varphi''''_{00}, \tag{21a}$$

$$\psi_{01} = \tfrac{1}{2}z(c - z)(\varphi'''_{00} - \varphi'_{01}), \tag{21b}$$

$$u_{01} = (\tfrac{1}{2}c - z)(\varphi''_{00} - \varphi_{01}), \tag{21c}$$

$$\theta_{01} = \varphi''_{00} - \varphi'_{01}. \tag{21d}$$

Here it has been assumed that $\sigma_{01} = 0$, meaning that the total heat transfer to an air column is contained in the zero order solution, while the first order heating, q_{01}, maintains a zero vertical lapse rate in θ_{01}.

Using the function φ_{00} derived in Subsection 2.2.1, we have computed φ_{01} and φ'_{01} numerically from eq. (21a), and then ψ_{01}, u_{01} and θ_{01} from eqs. (21b)–(21d). The values are shown in Fig. 10. As expected, the u_{01} wind is not in complete geostrophic balance with the corresponding temperature. The ageostrophic character of the total wind, $u_0 = u_{00} + \delta u_{01}$, may be evaluated directly from the momentum equation for this level of approximation;

$$\delta u_{oyy} + u_0 = -p_{oy},$$

where p_o is the non-dimensional pressure and eq. (8b) has been used to eliminate v_o. For small δ the first term may be approximated by the geostrophic wind, and it is not difficult to verify the general appearance of the diagrams in Fig. 10. An important result is a sharpening of the surface trough, measured by the vorticity. Not surprising, this is combined with an increase in the vertical circulation. The effect on the temperature is seen to be a strengthening of the temperature contrast over the land and a weakening over the sea.

2.2.3. Approximate solution for $\varepsilon \ll 1$. Turning now to the first order solution in ε we insert $u = u_{00} + \varepsilon u_{10} + \cdots$, and so forth, in eqs. (7a)–(7e), and get

$$v_{10y} + w_{10z} = 0, \tag{22a}$$

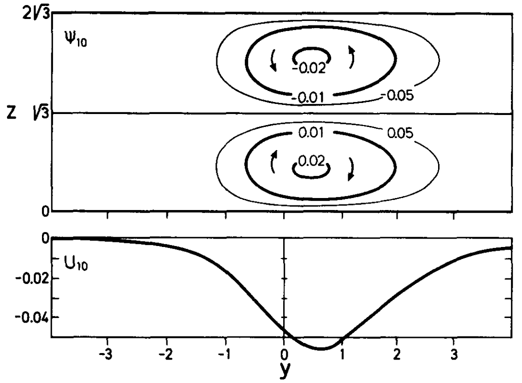

Fig. 11. First order solution in ε. Top plate shows stream function, while bottom plate is wind perturbation which is independent of z in this case. Temperature perturbation is zero. See text for further explanation.

$$-u_{10y} - v_{10} = -v_{00}\,u_{00y} - w_{00}\,u_{00z}, \tag{22b}$$

$$u_{10z} + \theta_{10y} = 0, \tag{22c}$$

$$-\theta_{10y} = \varphi_{10}(y), \tag{22d}$$

$$\varphi_{10}(y) = q_{10} - w_{10} - v_{00}\,\theta_{00y} - w_{00}\,\theta_{00z}, \tag{22e}$$

where the last term in eq. (22e) vanishes because $\theta_{00z} = 0$. Clearly, this solution contains some of the non-linear effects. We proceed as before, assuming $\sigma_{10} = 0$, and find after some arithmetic that

$$\varphi_{10}'' - \varphi_{10} = 0,$$

giving $\varphi_{10} = 0$ as the only solution which is finite at any y. Then it is seen from eqs. (22c) and (22d) that θ_{10} equals a constant which we choose to be zero, while u_{10} may be any function of y. This function, together with w_{10} and v_{10} (or ψ_{10}) is determined from eqs. (22a), (22b) and (22e), and turns out to be

$$\psi_{10} = \tfrac{1}{6} z(z-c)\left(z - \frac{c}{2}\right)(2\varphi_{00}'^2 - \varphi_{00}\,\varphi_{00}''), \tag{23}$$

$$u_{10} = -\varphi_{00}\,\varphi_{00}'. \tag{24}$$

The values corresponding to eq. (20) are pictured in Fig. 11. The prominent result of considering the non-linear terms appears to be the additional negative wind parallel to the coast. This wind is the same at all heights and has the strongest value slightly off the coast. There is no associated perturbation in the temperature. Since the thermal wind equation (22c) is satisfied, a horizontal pressure gradient in geostrophic balance with the wind may be postulated as in Fig. 9.

Obviously, the surface trough, measured by the vorticity is strengthened over the continent and weakened over the sea. Both the wind field and the transverse circulation shows a slight displacement towards the ocean in relation to the zero order solution. When the stream functions are added there appears to be a slight tendency towards a "tilt" in the familiar way, that is in the same direction as the vector lines for absolute vorticity (Eliassen, 1959).

2.3. *Solution for $\delta \simeq 1$*

We now return to eq. (15) and begin by discussing the case $\delta < 1$, but not necessarily small. The equation may be solved numerically in the same way as eq. (21a) with σ_0 as in eq. (19), and the result compared to the solution $\varphi_{00} + \delta\varphi_{01}$ derived earlier by series expansion. It turns out that the latter is a good approximation to the solution of eq. (15) provided δ is not larger than $\frac{1}{4}$. For still larger values of δ, the solution adjusts asymptotically to $(\sigma_0 + \sigma_0'')/c$, obtained by putting $\delta = 1$ in eq. (15).

Having solved the problem for the function φ_0, we may derive w_0 from eq. (11) and similar equations for the other variables. For instance, u_0 is determined by the equation

$$u_0 + \delta u_{0yy} = (z - c/2)\,\varphi_0. \tag{25}$$

Here we use as boundary conditions that u_0, in accordance with σ_0, is zero at $y = -\infty$ and finite at $y = +\infty$. The solution may be written as:

$$u_0 = (z - c/2)\,k \int_{-\infty}^{y} \varphi_0(\eta) \sin k(y-\eta)\,\mathrm{d}\eta, \tag{26}$$

where $k = \delta^{-1/2}$. It is not obvious that this solution has eq. (18c) as its limit as $k \to \infty$. That this is the case can be proven by integrating by parts, giving

$$u_0(y)(z - c/2)^{-1} = \varphi_0(y) - \lim_{\eta \to -\infty} \varphi_0(\eta)\cos k(y-\eta) + \int_{-\infty}^{y} \varphi_0'(\eta)\cos k(y-\eta)\,\mathrm{d}\eta. \tag{27}$$

As $k \to \infty$, the first term on the right hand side approaches $\varphi_{00}(y)$ and the Dirichlet integral becomes zero. The second term is also zero if $\varphi_0(\eta)$ vanishes as $\eta \to -\infty$, which has been postulated earlier.

When $\delta > 1$, the left-hand side of eq. (15) changes character, but it is still possible to find solutions which vary continuously with δ in the vicinity of $\delta = 1$. However, we shall not here make any effort to study these solutions closely. We have already pointed to the fact that according to eq. (5), the characteristic value of u is inversely proportional to $|\bar{v}|$ for a given value of the heating. With reference to the example discussed in Subsection 2.1, we conclude that for realistic values of the heating rate, the perturbation will be small for values of δ around one.

3. The influence of topography and boundary layer friction

We now return to the question of more refined lower boundary conditions mentioned in Subsection 2.2. For brevity we restrict the discussion to the asymptotic solution of Subsection 2.2.1.

From eqs. (17a)–(17d), one gets

$$w_{00zz} = \varphi''_{00}, \tag{28}$$

which is seen to be eq. (9) without the term containing δ. Using now as upper boundary conditions $w_{00}(z = c) = 0$, eq. (28) integrates to

$$w_{00} = \tfrac{1}{2} z(z - c)\varphi''_{00} - \frac{1}{c}(z - c) w_B, \tag{29}$$

where w_B must be derived from the topographic profile and the surface friction. We shall study these two effects separately in the following subsections, but first we shall pay some attention to the upper boundary condition. The use of $w_{00} = 0$ at top of the heated layer does not necessarily apply in this case. The reason is that the forcing does not come only from the heating in the convective layer but also from the lower boundary. The problem is rather difficult and we do not find it appropriate to get involved in models of more complicated structure in this study. Instead, we shall discuss briefly the conditions under which we may assume, as in eq. (29), that the vertical velocity is zero at the top of the convective layer, even if additional forcing from the lower boundary is present.

Looking at the second case study, and specifically at Fig. 6, we note a very strong inversion on the top of a layer with low stability. Intuitively it might be expected that the inversion suppresses the vertical movement. That this actually is so may be inferred from the equation for the upper layer,

$$w_{00zz} + s^2 w_{00yy} = 0$$

derived from eqs. (17) with $q_{00} = 0$ and no constraint on the temperature change. Here s^2, defined in eq. (3a), is retained, partly because the length scale may be imposed by the lower boundary, and partly because we want to consider a static stability which varies vertically. The equation, in fact, corresponds to the so-called omega equation. The appropriate solution equals w_c at $z = c$ and approaches zero as z increases, and must be fitted continuously and with continuous derivatives to a linear solution in the convective layer below $z = c$. It can be shown that w_c is small compared to w_B if s^2 is large.

Turning now to the first case study we note that the inversion on the top of the convective layer is much weaker, and that the atmosphere above is not very stable either. Therefore, in this case the assumption of zero vertical velocity on top of the heated layer may not be very satisfactory. However, this case is somewhat special, and in most cases we have studied, the middle troposphere is much more stable.

3.1. *The topography*

The vertical velocity at the ground may be written in dimensional form as

$$w_M = (\bar{v} + v(y, h))\, h'. \tag{30}$$

Here h is the height of the ground, considered to be a function of y with a derivative which we write as h'. We also use the approximation $v(y, h) \simeq v(y, 0)$, assuming, in fact that $\mu = H_M/H \ll 1$, where H_M is the scale height of the topography. When eq. (30) is made non-dimensional, using as before $W = VH/L$ and $V = \varepsilon|\bar{v}|$, it becomes

$$w_M = \frac{\mu}{\varepsilon}(-1 + \varepsilon v(y, 0))\, h'. \tag{31}$$

Obviously, if $\varepsilon \ll 1$, the second term in the parenthesis may be neglected, and then the topographic influence is independent of the perturbation caused by the heating. In fact, it depends only on the basic state wind component across the sloping topography. Since this problem has been studied in numerous papers, we shall not linger over it here. The general result is known to be anticyclonic vorticity over a mountain range. However, for the purpose of the following discussion we shall at this point mention some general consequences of eq. (29).

Repeating the procedure leading to eq. (17f), one gets in the present case

$$\varphi_{00}'' - \varphi_{00} = -\frac{\mu}{2\varepsilon} h'. \tag{32}$$

We have here omitted the forcing σ_{00}/c, caused by the heating, since this effect can be treated independently. Eq. (32) may be solved in principle since h' is known. Then, w_{00} is determined from eq. (29) with $w_B = -(\mu/\varepsilon) h'$. The influence of the sloping terrain, contained in the last term, has its maximum at the earth's surface and decreases linearly to zero at the model top. The other part is the vertical component of a secondary circulation which in this case is caused by the heating/cooling of the stable air mass when moved vertically by the influence of the terrain. The secondary vertical velocity is zero at the earth's surface and at the model top, obtaining its largest absolute value at middle height. Considering the structure of the solution, which is similar to eq. (18a), it may be shown that the two parts of the vertical velocity in general counteract at middle heights. Moreover, since the solution has an intrinsic scale equal to the Rossby radius, its influence may extend beyond the area of elevated ground and be present even over the ocean. We shall see examples of this later in connection with the surface friction.

For the reason of clarity we mention again that this result is a consequence of the constraint that φ in eqs. (7d) and (7e) is a function of y only. Also note that the above deduction is strictly true only for the asymptotic solution of Subsection 2.2.1. In fact, it may be shown to be a consequence of the exact geostrophic balance.

3.2. *Surface friction*

As mentioned earlier the influence of surface friction will be parameterized by means of Ekman layer theory. In large-scale dynamics, the Ekman layer is often tacitly assumed to be below the lower boundary of the model, where it imposes a vertical velocity proportional to the relative vorticity. In the present case it is obvious that the vertical momentum flux and the heat flux in the convective layer cannot be separated physically, so that the Ekman layer clearly is contained inside the model as we have defined it. However, an Ekman layer solution in the classical form may still be applied if the Ekman layer height, defined by eq. (34) below, is small compared to the model height, meaning that the Ekman volume flux is confined to the lowest part of the model.

According to Charney and Eliassen (1949), the horizontal flux across the isobars may be written

$$F_E = H_E(\bar{u} + u), \tag{33}$$

where H_E, in the present paper referred to as the Ekman layer height, is defined as

$$H_E = (2K/f)^{1/2} \sin\alpha \cos\alpha. \tag{34}$$

Here K is the eddy viscosity and α the angle between the isobars and the wind direction in the surface layer. Both K and α may have different values over the ocean and over the continent. Thus, H_E in general varies with the y coordinate.

By means of the continuity equation, the vertical velocity imposed by the Ekman layer flux convergence may in non-dimensional form be expressed as

$$w_E = -\frac{\varepsilon\kappa}{\delta^{1/2}} \frac{\partial}{\partial y} ((\bar{u} + u(y, 0)) b(y)). \tag{35}$$

Here, $b(y) = H_E/H_E^*$, H_E^* being the characteristic value of H_E, and $\kappa = H_E^*/H$, the Ekman number. Furthermore, $\bar{u}$ and u have both been scaled by U. Assuming H_E^* to be 200 m, κ is characteristically of size 0.1. The combined non-dimensional constant, $\varepsilon\kappa/\delta^{1/2}$, depends on ε and δ in such a way that a strong perturbation (ε large) or a weak on-shore wind (δ small) makes the constant large, and accordingly increases the influence of the surface friction. In Subsection 2.1, it was noted that ε and $\delta^{1/2}$ tend to be inversely proportional. Therefore, a small $\bar{v}$ generally makes the constant large. For simplicity, however, we shall here study only cases in which $\delta^{1/2}$ is not much smaller than ε. If convenient, we may then perform a series expansion in powers of the constant.

Inserting from eq. (35) into eq. (29), one gets

$$w_{00} = \tfrac{1}{2} z(z-c)\varphi''_{00} + \frac{\varepsilon\kappa}{\delta^{1/2} c}(z-c) \times \left(\left(\bar{u} - \frac{c}{2}\varphi_{00}\right) b\right)', \tag{36}$$

where $u(y,0)$ in eq. (35) has been replaced by $-(c/2)\varphi_{00}$ from eq. (18c). Following the same procedure as before, we obtain the equation for φ_{00};

$$\varphi''_{00} - \varphi_{00} - \frac{\varepsilon\kappa}{\delta^{1/2}} \frac{c}{4} (b\varphi_{00})_y = -\frac{1}{c}\sigma_{00} - \frac{\varepsilon\kappa}{\delta^{1/2}} \frac{\bar{u}}{2} b'. \tag{37}$$

If b is a known function of y, this equation must in general be solved numerically. For b equal to a constant, a solution similar to eq. (18a) is easily established. However, we find it more enlightening to proceed by series expansions in the small number $\varepsilon\kappa/\delta^{1/2}$. Accordingly, we attempt to find solutions of eq. (37) in the form

$$\varphi_{00} = \varphi_{000} + \frac{\varepsilon\kappa}{\delta^{1/2}}\varphi_{001} + \cdots. \tag{38}$$

Inserting in eq. (33), the zero order terms give

$$\varphi''_{000} - \varphi_{000} = -\frac{1}{c}\sigma_{00}, \tag{39}$$

which is identical to eq. (17f) and reproduces the results eqs. (18a)–(18f). The first-order equation reads

$$\varphi''_{001} - \varphi_{001} = (c/4)(b\varphi_{000})' - (\bar{u}/2)b'. \tag{40}$$

This equation will be solved in two special cases. First we assume that $b = 1$, which makes the second right-hand side term zero. This implies investigating the influence of a homogeneous surface on the perturbation. Later, we discuss a specific case where b changes at the coast.

3.2.1. Constant Ekman height. Since $b = 1$, the first-order equation becomes

$$\varphi''_{001} - \varphi_{001} = (c/4)\varphi'_{000}. \tag{41}$$

We may then derive corresponding solutions for the other variables, starting with

$$w_{001} = \tfrac{1}{2} z(z-c)\varphi''_{001} - \tfrac{1}{2}(z-c)\varphi'_{000}. \tag{42}$$

Here the last term (multiplied by $\varepsilon\kappa/\delta^{1/2}$) is seen to be the vertical velocity resulting from the Ekman layer convergence, while the first right-hand side term represents a secondary circulation similar to the one discussed in Subsection 3.1.

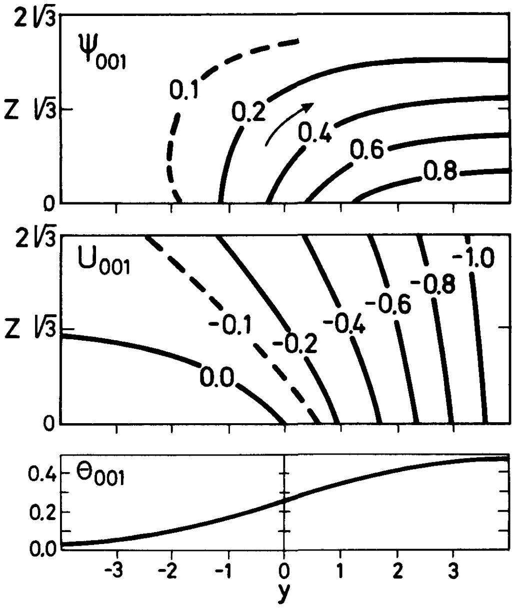

Fig. 12. Correction to the asymptotic solution (Fig. 8) caused by homogeneous friction. See text for further explanation.

From eq. (42) and the continuity equation, one gets

$$v_{001} = -(z - c/2)\varphi'_{001} + \tfrac{1}{2}\varphi_{000}, \tag{43}$$

where a constant has been chosen so as to give $v_{001}(-\infty, z) = 0$, in agreement with earlier assumptions. Solutions for u_{001} and θ_{001}, consistent with eqs. (42) and (43) are easily derived.

Choosing σ_{00} as in eq. (19), we have computed ψ_{001}, u_{001} and θ_{001}. Values are pictured in Fig. 12, and demonstrate that the boundary layer convergence into the trough flows towards the ocean at upper levels, a consequence of the lateral boundary condition we have chosen in eq. (43). The corresponding u_{001} is seen to produce increasing vorticity towards the positive y-direction, thus in general making the trough less sharp.

3.2.2. Variable Ekman height. In this case, eq. (40) applies in its complete form. However, considerable insight into the dynamics may be gained by studying a somewhat simpler case. First, we note that the basic state wind component parallel to the coast, $\bar{u}$, occurs only in the last term, where it has been scaled by U. However, this scale has been derived basically from the heat fluxes. Therefore, we do not know for sure that the non-dimensional $\bar{u}$ has the characteristic size of unity, since we have placed no restriction upon this wind component as yet. On this background we find it necessary to study the case where the basic state wind is so strong or the heating so weak that the last term in eq. (40) dominates, and the first right-hand term, therefore, may be neglectred. Then we are left without an appropriate definition of U. Such a definition must be derived from the vertical velocity forced by $\bar{u}$ and the variation of b across the coast. Furthermore, if we want to study the asymptotic case, we must make sure that the U so defined is so small that $\varepsilon \ll 1$.

We begin by writing eq. (35) in dimensional form as

$$w_E = -\bar{u}B', \tag{44}$$

where $B = (2K/f)^{1/2} \sin\alpha \cos\alpha$ and where we have neglected $u(y, 0)$ compared to $\bar{u}$. We assume that B changes from a value B_1 over the ocean to a larger value, B_2, over the continent. Then, in agreement with previous lateral boundary conditions, we may approximate the volume flux at large y as

$$VH = |\bar{u}|(B_2 - B_1). \tag{45}$$

From this equation, the scale V may be derived, provided that H may be determined. Finally, if $\varepsilon \ll 1$, one gets from eq. (1b)

$$|\bar{v}|\, U/L = f|\bar{u}|(B_2 - B_1)/H \tag{46}$$

or

$$\varepsilon = \kappa|\bar{u}|/|\bar{v}|, \tag{47}$$

where $\kappa = (B_2 - B_1)/H$. From eq. (47), we can derive a condition for $\varepsilon \ll 1$. Note that κ, in accordance with previous evaluations is of order 0.1.

We now return to eq. (40), which we write as:

$$\varphi''_{001} - \varphi_{001} = -\frac{\bar{u}}{2} b', \tag{48}$$

with the solution

$$\varphi_{001} = \frac{\bar{u}}{4} \int_{-\infty}^{\infty} e^{-|y-\eta|} b'(\eta)\, d\eta. \tag{49}$$

It appears mathematically simple and physically plausible to assume that b changes abruptly at the coast. Accordingly, we postulate $b' = -\delta(y)$, where the delta function is defined as

$$\delta(y) = \lim_{k\to\infty} \frac{k}{2\cosh^2 ky}. \tag{50}$$

Correspondingly, b is chosen as

$$b = 1 - \frac{1}{2} \lim_{k\to\infty} \tanh ky, \tag{51}$$

implying that b increases from $\frac{1}{2}$ to $\frac{3}{2}$ from the ocean to the continent. This definition leads to the following solution

$$\varphi_{001} = -\frac{\bar{u}}{4} e^{-|y|}. \tag{52}$$

Corresponding solutions for the other variables depend on boundary conditions which must be specified. As before, we postulate that the variables vanish for large negative y. Then

$$\theta_{001} = \int_{-\infty}^{y} -\varphi_{001}(\eta)\, d\eta = \begin{bmatrix} \bar{u}/2 + \varphi_{001}, & y > 0, \\ -\varphi_{001}, & y < 0. \end{bmatrix} \tag{53}$$

The other variables, derived successively from equations similar to eqs. (17a)–(17c), are

$$\psi_{001} = \begin{bmatrix} -z(z-c)\varphi_{001}/2 - (z-c)\bar{u}/c, & y > 0, \\ z(z-c)\varphi_{001}/2, & y < 0, \end{bmatrix} \tag{54}$$

$$u_{001} = (z - c/2)\varphi_{001} + \begin{bmatrix} -y\bar{u}/c & y > 0, \\ 0 & y < 0. \end{bmatrix} \tag{55}$$

The stream function, φ_{001}, is discontinuous at $y = 0$, reflecting the fact that the vertical flux from the Ekman layer convergence/divergence is restricted to an "infinitely narrow strip" along the coast.

The solutions eqs. (54), (55) and (53) are pictured in Fig. 13 for $\bar{u} = 1$. The streamlines are drawn approximately as they would look if the vertical velocity at the coastline was large, but finite. The top picture represents the primary flow from the Ekman layer while the middle picture shows the secondary circulation (the Ekman layer is not indicated). Finally, the bottom diagram shows the isolines for u_{001} (continuous) and for θ_{001} (broken). There is a wind maximum ("low level jet") along the coast in direction of the positive x-axis, and a

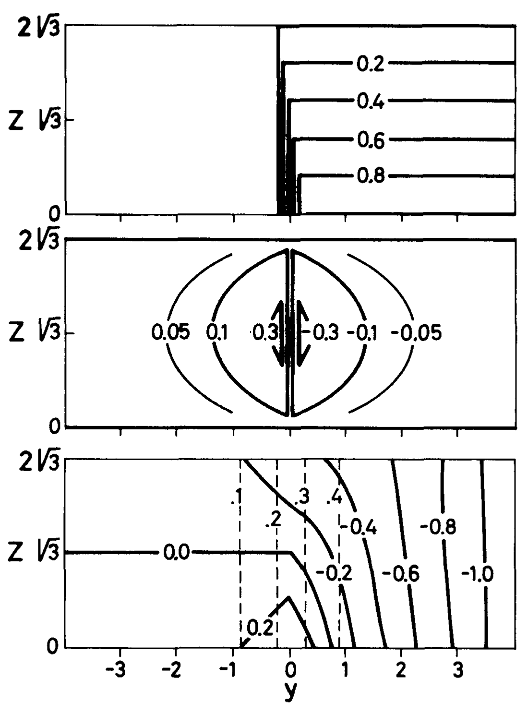

Fig. 13. Perturbation of the basic state wind and temperature caused by an abrupt change in the drag coefficient at the coast. See text for further explanation.

horizontal temperature gradient at all levels pointing in the positive y-direction. For $\bar{u}$ negative the wind direction and temperature gradient is reversed. As mentioned before, the secondary circulation produces a downward motion where the Ekman layer convergence gives upward motion. However, the two flows vary differently with height, so that the resulting vertical velocity is strong at low levels but weak at high levels. We also point to the fact that the secondary circulation induces a compensating motion which covers an area of characteristic dimension as the deformation radius. The total motion in a cross section, which is derived by adding the two stream functions, shows fan-shaped streamlines coming out of the Ekman layer (at $z = 0$) and curving towards the right.

3.2.3. Comparison with the case studies. We conclude the study of the frictional effects by applying the model results to the case studies, and begin with the trough pictured in Fig. 1, presumably caused primarily by differential heating. In order to apply our results with confidence, we must assume that the heating is weak enough to allow us to neglect $\bar{u}$ compared to u in eq. (35) and that ε given by eq. (47) is small. In agreement with the case study related to Fig. 1, we assume that $\bar{u} < 0$. Then, there will be a suction of air into the Ekman layer along the coast, giving divergence at low levels. The secondary circulation produces sinking motion over an extended area on both sides of the coastline. The additional u velocity shows a low level maximum of anticyclonic vorticity just outside the coast which weakens the trough caused by the heating. Also, the temperature gradient caused by the friction has opposite direction to the one associated with the heating. So, by and large, the friction weakens both the trough and the temperature contrast.

The second case study (Fig. 5) is quite different. Here $\bar{u} > 0$, which leads to convergence in the Ekman layer and upward motion along the coast. There will be increased cyclonic curvature of the isobars over the ocean (Fig. 13, bottom plate). If we had chosen the arbitrary constants otherwise, we could have arranged to have the air from the Ekman layer flowing in both the positive and the negative y-direction. This would have given anticyclonic vorticity over the continent, in still better agreement with this particular case study.

Still more spectacular is the observed wind maximum at the coast which fits well with the model study. (The associated pressure gradient cannot be analysed correctly because of the long distance between the observing stations.) The temperature gradient predicted by the model, increases the temperature difference between the sea and the cold land and, in addition, the Ekman layer convergence strengthens the contrast in the boundary layer. In summary, there seems to be ample reason for a coastal front in this case.

The map pictured in Fig. 5 shows maximum precipitation at the coastal stations, a fact noted by Bergeron (1949). However, there is also precipitation on the inland stations, which Bergeron attributed to the gradually sloping terrain. We believe that it might in part be caused by the secondary circulation, which Bergeron was not aware of. In fact, the model also predicts the possibility of precipitation over the sea, within a distance of about one Rossby radius.

4. Concluding remarks

Our effort to find stationary solutions was dictated by the fact that configurations like those pictured in Fig. 1 and Fig. 5 could last for days. The leading idea has been that the change in the heating rate and the surface friction were the dominating factors in tying the perturbation to the coast. However, the perturbation cannot be independent of the general synoptic picture. A very cold air mass is, of course, necessary in order to make the heating rate large. In addition, our analysis has shown that there is an upper limit to the value of the on-shore basic state wind.

Similar considerations apply to the lateral boundary conditions. As previously stated, the uniqueness of the solution requires boundary conditions along two "walls" parallel to the coastline. We have chosen these conditions somewhat arbitrarily, but has to some extent been led by the study of characteristic cases. For instance, the trough has been assumed to vanish over the continent at large distance from the coast, while over the ocean the requirement has been that the variables remain finite. This has not been possible in all cases. Specifically, when considering friction, we were forced to accept that the perturbation wind parallel to the coast increased steadily with increasing distance. Moreover, the choice of the basic state has proved to be rather restrictive. This is demonstrated by the asymptotic solutions pictured in Fig. 8 and Fig. 9, where the additional wind parallel to the coast, although remaining finite, approaches a constant value at infinity. To overcome this difficulty we suggested that the ice-edge may provide a suitable boundary. Probably this indicates that a general turning of the large scale wind over the ocean may help to develop the trough. Or, in other words that a large-scale trough, independent of the coast, may be necessary, or at least desirable.

Since we have deliberately chosen to make several simplifying assumptions, it may perhaps be said that we have, in some respect, chosen our result in advance. One example is the character of the "heating" function in eq. (19), where the horizontal scale is chosen to be the Rossby deformation radius. This is partly done for computational convenience, but also because a realistic parameterization would have made our approach quite impossible. A change to a shorter horizontal scale (one half of the above value) has been tried, but did not make much change in the general character and size of the solution.

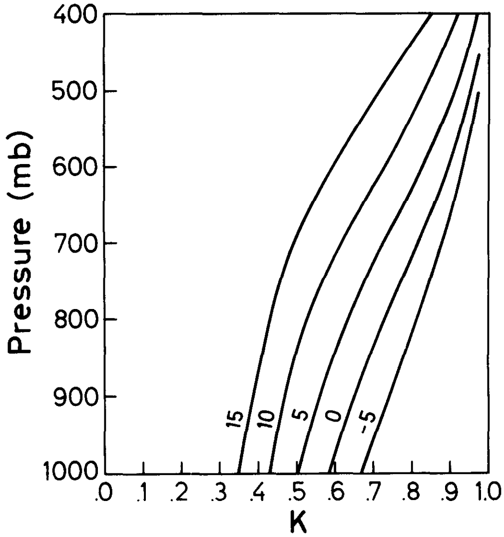

Fig. 14. The ratio $K = \delta\theta/\delta\theta_e$ along some saturated adiabats (θ_e = constant). The adiabats are defined by their 1000 mb temperature (in degrees centigrade). See text for further explanation.

Some of our results appear to be quite obvious. Others are not. For instance, if the perturbation velocity parallel to the coast is assumed to be geostrophic, the general appearance of the trough may be explained by the geostrophic wind relation since the horizontal temperature gradient is known in its broad feature. However, the vertical circulation and the influence from the non-linear terms and departure from geostrophic balance, may not be fully understood without considering the complete set of equations.

5. Acknowledgements

This study has received financial support from The Norwegian Meteorological Institute as a part of The Polar Lows Project. Thanks are due to Anne Line Skaland for typing the manuscript.

6. Appendix

Heating of a saturated adiabatic layer

We take as starting point the assumption that the lapse rate in a moist convective layer is approximated with sufficient accuracy by the saturated adiabat. When the layer is heated, the approximation must continue to be valid, only the saturated adiabat must be a different one. If the adiabat is defined by a specific value of the equivalent potential temperature, θ_e, the problem we shall consider is the following: Let θ_e be increased by the small value $\delta\theta_e$. What is the corresponding change in the potential temperature, $\delta\theta$?

For our purpose, it suffices to use the well known approximate definition of θ_e, i.e.,

$$\theta_e = \theta \exp(Lr/c_p T), \tag{A1}$$

where T and r are the saturation temperature and mixing ratio. Then, at constant pressure

$$\delta\theta_e/\theta_e = \delta\theta/\theta + (\delta r/T - r\,\delta T/T^2)\,L/c_p. \tag{A2}$$

In this equation, we substitute for δr by:

$$\delta r = \varepsilon L r\,\delta T/RT^2, \tag{A3}$$

obtained from the Clausius–Clapeyron equation, $\delta T/T$ by $\delta\theta/\theta$ and θ_e by (A1). Then

$$\delta\theta/\delta\theta_e = (1 + Lr(\varepsilon L/RT - 1)/c_p T)^{-1} \times \exp(-Lr/c_p T). \tag{A4}$$

From this equation, $K = \delta\theta/\delta\theta_e$ may be computed as function of pressure on any specific saturated adiabat. The appropriate values of r and T may conveniently be derived from a thermodynamic diagram or looked up in a table.

Fig. 14 shows the variation of K along some saturated adiabats, defined by their 1000 mb temperature. As may be verified by using eq. (A4), K approaches 1 asymptotically as p decreases. The largest variation of K is at large pressure and large 1000 mb temperature. A characteristic 1000 mb temperature is 0°C for the case under investigation. This gives an increase of K from 0.58 at 1000 mb to 0.72 at 800 mb. If, in addition it is taken into consideration that $\delta\theta$ has no variation below the condensation level, the model assumption of a constant $\delta\theta$ is acceptable, considering the other approximations used in formulating the model.

REFERENCES

Ballentine, R. J. 1980. A numerical investigation of New England coastal frontogenesis. *Mon. Wea. Rev. 108*, 1479–1497.

Bergeron, T. 1949. The problem of artificial control of rainfall on the globe. II. The coastal orographic maximum of precipitation in autumn and winter. *Tellus 1*, 3, 15–33.

Bosart, L. F., Vando, C. J. and Helsdon, J. H. Jr. 1972. Coastal frontogenesis. *J. Appl. Met. 11*, 1236–1258.

Bosart, L. F. 1975. New England coastal frontogenesis. *Quart. J. R. Met. Soc. 101*, 957–978.

Charney, J. G. and Eliassen, A. 1949. A numerical method for predicting the perturbations of the middle latitude westerlies. *Tellus 1*, 2, 38–54.

Eliassen, A. 1959. On the formation of fronts in the atmosphere. *The Rossby Memorial Volume*, Rockefeller Institute and Oxford University, New York, 227–287.

Eliassen, A. 1962. On the vertical circulation in frontal zones. *Geof. Publ. 24*, 148–160.

Økland, H. 1983. Modelling the height, temperature and relative humidity of a well-mixed planetary boundary layer over a water surface. *Boundary-Layer Meteorol. 25*, 121–141.

Økland, H. 1987. Heating by organized convection as a source of polar low intensification. *Tellus 39A*, 397–407.

Uccellini, L. W., Petersen, R. A., Brill, K. F., Kocin, P. J. and Tuccillo, J. J. 1987. Synergistic interaction between an upper-level jet streak and diabatic processes that influence the development of a low-level jet and a secondary coastal cyclone. *Mon. Wea. Rev. 115*, 2227–2261.